MDPI

Article

Friction and Wear Reduction of Tungsten Carbide and Titanium Alloy Contacts via Graphene Nanolubricant

Chris Goralka [1], **Jake Bridges** [1], **Muhammad Jahan** [1], **Mark Sidebottom** [1], **Timothy Cameron** [1], **Yan Lu** [2] and **Zhijiang Ye** [1,*]

[1] Mechanical and Manufacturing Engineering, Miami University, 501 E. High St., Oxford, OH 45056, USA
[2] Key Laboratory of Metallurgical Equipment and Control Technology, Wuhan University of Science and Technology, Wuhan 430081, China
[*] Correspondence: zye@miamioh.edu

Abstract: The tribological behavior of graphene as an additive in a water-based nanofluid lubricant was investigated using pin-on-disk tests on titanium alloy (Ti-6Al-4V) and cemented tungsten carbide (WC–Co) contacts. The effect of graphene concentration and surface roughness was investigated. A non-monotonic trend of friction and wear with increasing concentration was observed. An optimal graphene concentration of 0.10 wt.% was found to provide the lowest friction and wear at different surface roughnesses, with the friction, specific wear rate of the sample surface, and tip wear reduced by 29%, 37%, and 95%, respectively. The friction reduction and anti-wear performance of the nanofluids increased as the sample surface roughness increased. The non-monotonic friction and wear trends can be explained by the agglomeration of graphene around the contact zone, where too small a graphene concentration does not provide enough lubrication and too high a concentration prevents sliding owing to a large amount of agglomeration particles at the contact. The superior friction and wear performance of the graphene nanolubricants demonstrate its potential in minimum quantity lubrication (MQL) and other applications.

Keywords: graphene; titanium alloy; surface roughness; friction; wear

1. Introduction

Titanium and its alloys have significant applications in aerospace engineering, biomedical engineering, sports applications, electronics, and high-end automotive systems, thanks to the materials' very high tensile strength and toughness, extraordinary corrosion and heat resistance, relative light weight, and excellent biocompatibility. One of the most commonly used titanium alloys is Ti-6Al-4V (Grade 5). It has widespread use in the aerospace, marine, and biomedical industries. However, the properties of Ti-6Al-4V (high toughness, work hardening, and a tendency to produce continuous chips) often lead to high friction and accelerated tool wear [1–5]. Additionally, Ti-6Al-4V has poor thermal conductivity, which leads to high temperatures in the cutting tool tip [6]. The elevated temperature at the surface oxidizes the Ti-6Al-4V workpiece and tool tip, which leads to embrittlement of the workpiece and reactions with the tool material. The embrittlement and chemical reactions can cause adhesion that negatively impacts tool life [7].

To minimize friction, wear, and heat from the tool tip, flood cooling is commonly used when machining titanium alloy. In flood cooling, a large amount of coolant floods the work zone, absorbing heat and washing away chips. However, flood cooling is costly and has a high environmental risk [8]. Typical flood coolants are mineral oils mixed with water and other additives; workpieces must be cleaned after machining, fluid must be disposed of in a way that does not cause environmental harm, and fumes created can negatively impact worker health. The large amount of coolant needed, along with post-machining cleanup, typically accounts for ~20% of the total manufacturing cost [9]. Minimum quantity

lubrication (MQL) presents an alternative to flood cooling. In MQL, a small amount of fluid is sprayed directly onto the tool tip while cutting. Costs are lower as the amount of fluid needed is greatly reduced and cleanup is not required owing to most of the fluid evaporating during machining. Dorr and Sahm found that MQL reduced machining costs at BMW by 22% compared with conventional cooling [10]. Water and vegetable oil may replace mineral oils as the base of these lubricants, which conforms to green machining guidelines. However, highly effective MQL lubricants are needed for hard-to-machine materials such as titanium alloys. Nanofluids have been proposed as a possible solution and have shown great potential in machining titanium alloys.

Nanofluids are the suspension of solid nanoparticles within a fluid. These nanoparticles augment the friction and heat transfer characteristics of the base fluid [10]. Recent research has been carried out on the use of two-dimensional (2D) materials, such as graphene (G), molybdenum disulfide (MoS2), and boron nitride (BN), in nanofluid lubricants [9,11–14]. However, most studies have focused on basic steel–steel contacts rather than Ti–WC contacts [9,11–14]. Graphene is an atom thick allotrope of carbon with a hexagonal lattice structure [15]. Graphene also has an atomically smooth surface, allowing easy shear over itself and low friction [16–18], as well as excellent thermal conductivity [10,15], which are valuable qualities for a nanofluid additive. Previous studies have shown effectiveness of graphene and graphene oxide as a lubricant additive for a wide variety of contacts [19–23], including MQL machining of titanium alloy [24–26]. However, there is still a lack of fundamental understanding on whether and how the friction and wear on Ti-6Al-4V is affected by applying graphene nanolubricants. To the best of the authors' knowledge, no previous studies have performed pin-on-disk tests to investigate the tribological behavior of graphene nanolubricants using MQL techniques on titanium alloy and tungsten carbide contacts. This will bring a deeper understanding of the potential improvements that graphene nanolubricants can bring to the production of titanium alloy.

In this study, we focus on the use of graphene as a nanofluid additive for Ti-6Al-4V and WC–Co contacts. WC–Co was chosen as the counterbody to Ti-6Al-4V owing to its common use in machining operations [2]. Specifically, the friction and wear of graphene nanofluids for titanium alloy and tungsten carbide contacts were evaluated using a pin-on-disk tribometer. The effects of graphene concentration and surface roughness of the materials in contact were investigated. The worn surfaces of both the titanium alloy and WC were analyzed using optical profilometry and electron microscopy to understand the nanofluids' lubrication mechanisms. Our study can provide insights into the fundamental understanding of nanolubricant performance on titanium alloys. This fundamental knowledge can be directly related and applied to that of MQL machining of titanium alloy with WC–Co machining tools.

2. Materials and Methods

2.1. Friction and Wear Experiments

The friction and wear experiments were performed via pin-on-disk tests using an RTEC multifunctional tribometer (MFT-5000), illustrated in Figure 1a. The multifunctional tribometer has a rotary drive (ball on disk) of speed range from 0.1 rpm to 5000 rpm with 0.1 rpm resolution. The force sensor has a range of 0.5 to 50 N with a resolution of 1.5 mN. The data acquisition rate is up to 200 kHz. A 6.35 mm cemented tungsten carbide ball was used as the pin, which is the same material as typical machining tool tips. The sample substrate is a Ti-6Al-4V disk with a 4-inch diameter. The surface roughness (Ra) of the sample substrates was controlled at 0.08, 0.51, and 1.02 μm, which are comparable to the roughness of machined work pieces. Roughness was varied to observe the effects different values of roughness had on friction and wear. Graphene–water nanolubricants were synthesized with concentrations of 0.05, 0.10, 0.15, and 0.25 wt.%. Graphene nanoflakes from Graphene Supermarket (Ronkonkoma, NY, USA) were combined with distilled water. Before each experiment, the graphene nanolubricants were placed in an ultrasonic bath for 30 min to ensure no aggregation of graphene within the solution. The graphene

nanolubricants were sprayed onto the sample surface, which mimics the condition for MQL machining. A normal load of 2 N (contact pressure of 770 MPa) was applied to the tip, while the Ti-6Al-4V disk slid against the pin at 50 mm/s for 15 min (sliding distance = 45 m).

2.2. Surface Characterization

Three-dimensional (3D) surface profiles were characterized using a Bruker Contour GT scanning white light interferometer (SWLI) before and after the experiments. Three-dimensional (3D) profiles of wear scars on both the Ti-6Al-4V Disk and WC pins were characterized and analyzed. These profiles were used to determine the worn volume within the wear scars as well as the roughness of each surface. The specific wear rate was calculated with Equation (1):

$$K = \frac{V}{F_n S} = \frac{2\pi R A}{F_n S} \tag{1}$$

where K is the specific wear rate (mm^3/Nm), V is the wear volume (mm^3), F_n is the normal force (N), S is the sliding distance (m), R is the wear track radius (mm), and A is the average cross-sectional area of the wear track (mm^2). To calculate the wear volume (V) of the Ti disks, the wear areas of four cross-sectional profile scans (A) were averaged and multiplied by the track circumference ($2\pi R$). The boundaries of the wear scars were visually identified in each cross-sectional area profile. Trapezoidal integration was performed between these bounds to determine the worn area at that location. To calculate the wear volume (V) on the WC pin, the positive (adhered) and negative (abraded) volume was measured from the 3D SWLI scans using pixel area and height. The curved pin surface was first flattened using a least-squares sphere fit of the unworn WC ball. The volume of the wear scar was then calculated by summing products of the pixel area and z-heights. Positive (adhered) volume was defined as the volume above the unworn surface, while negative (abraded) volume was defined as the volume below the unworn surface.

The law of propagation of uncertainty was used to determine the combined standard uncertainty for specific wear rate, $u_c(K)$, in Equation (2) [27–31]:

$$u_c{}^2(K) = \left(\frac{\partial K}{\partial V}\right)^2 u^2(V) + \left(\frac{\partial K}{\partial \underline{F_n}}\right)^2 u^2\left(\underline{F_n}\right) = \left(\frac{\partial K}{\partial A}\right)^2 u^2(A) + \left(\frac{\partial K}{\partial \underline{F_n}}\right)^2 u^2\left(\underline{F_n}\right) \tag{2}$$

where $u(V)$ is the standard uncertainty of wear volume, $u(\underline{F_n})$ is the standard uncertainty of time-averaged normal force, and $u(A)$ is the standard uncertainty in the cross-sectional wear area.

For all tests, instrument error was assumed to be negligible. For the disk wear tracks, error in the cross-sectional area was introduced through visual identification of wear track bounds. Disk surface roughness creates uncertainty in the vertical boundaries and width of the wear track. As proposed by Erickson et al. [31], this uncertainty was estimated using Equation (3):

$$u(A) = R_p w \tag{3}$$

where R_p is the maximum profile peak height of the unworn disk surface and w is the width of the wear track.

Additionally, a Zeiss Supra 35VP scanning electron microscope (SEM) was also used to analyze the structure and identify possible wear modes of the wear scars. Elemental analysis was performed with a Bruker Quantax 100 EDS system.

3. Results and Discussion

*3.1. Effect of Graphene Concentration on Friction and Wear*

Figure 1b shows the coefficient of friction (COF) as a function of graphene concentration. A non-monotonic friction trend was observed and 0.10 wt.% graphene provided the lowest COF of 0.29, which is a friction reduction of 29% compared with the dry test. The specific wear rate on the titanium alloy substrate was also reduced with graphene lubricants compared with lubricants without graphene, and a similar trend of wear versus graphene

concentration was observed, as shown in Figure 1c. A wt.% of 0.10 graphene showed the lowest wear rate of 4.8×10^{-4} mm^3/Nm, while pure water resulted in a wear rate of 7.1×10^{-4} mm^3/Nm. WC tip wear was also characterized and investigated. It is believed that friction and wear were not reduced more due to agglomeration of graphene particles, causing them to be too big to fill in abrasions on the substrate. As shown in Figure 2a, the pin from the distilled water only experiment has more visible wear than the pin from the 0.10 wt.% graphene experiment (Figure 2b). Abrasion and adhesion wear on pin was identified and characterized, as shown in Figure 2c. Distilled water resulted in 2.2×10^5 μm^3 of abrasion wear, while 0.10 wt.% graphene–water resulted in 1.1×10^4 μm^3 of abrasion wear (Figure 2c). The volume of the material adhered was also larger with distilled water only than with 0.10 wt.% graphene, at 8.0×10^4 and 7.5×10^3 μm^3, respectively. Figure 2c shows that the specific wear rate for the WC pin is 95% lower with 0.10 wt.% graphene–water than with distilled water at 1.2×10^{-7} and 2.4×10^{-6} mm^3/Nm, respectively. The COF value obtained from our study is comparable to previously reported results on graphene in deionized water [26] and is much lower than graphene-oxide-based lubricants [27]. The wear scar on the pin without graphene lubricant contains a large amount of titanium adhered from the disk. To confirm the wear materials, SEM characterizations and EDS analysis of the wear scar were conducted, confirming that titanium from the disk was welded to the pin (Figure 3a,b).
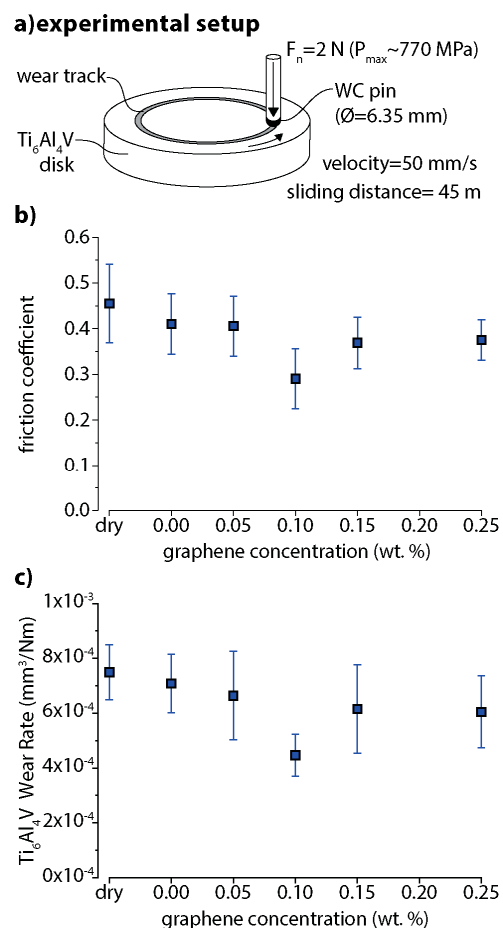

Figure 1. (**a**) Illustration of pin-on-disk experiment: WC tip sliding against titanium alloy disk. (**b**) Coefficient of friction for various concentrations of graphene nanoflakes in distilled water. (**c**) Specific wear rate of titanium alloy disk for various concentrations of graphene nanoflakes in distilled water. For (**b**,**c**): The leftmost data point is the dry condition. Error bars are standard uncertainty.
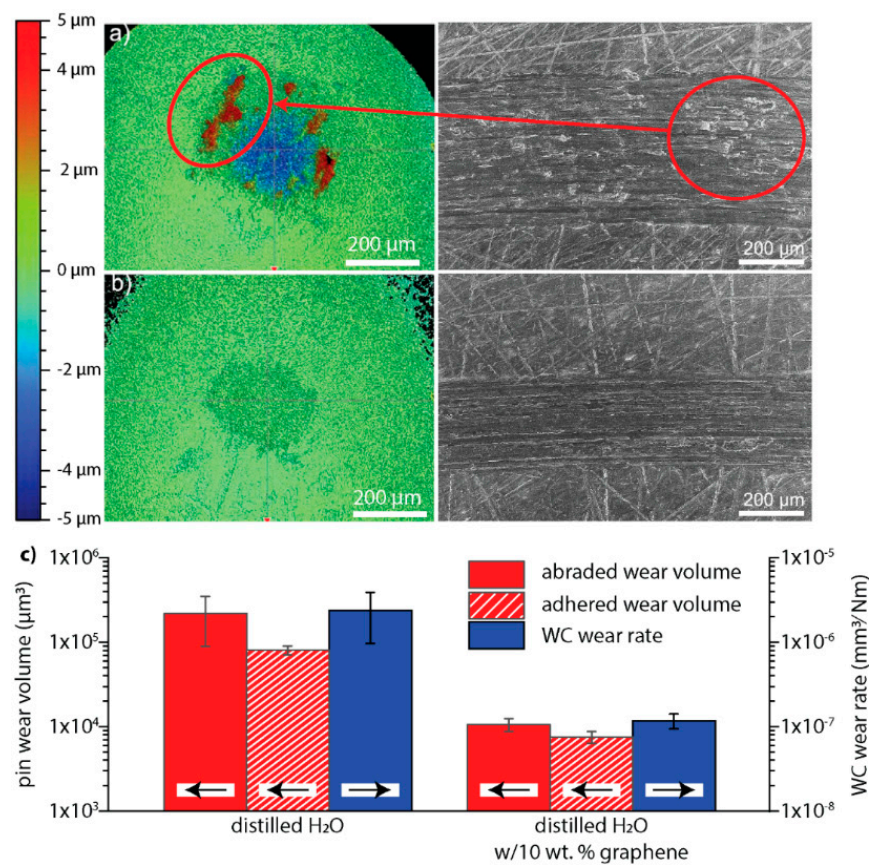
Figure 2. SWLI scan of pin wear scar (**left**) and SEM image of disk wear track (**right**): (**a**) distilled water only and (**b**) 0.10 wt.% graphene–water. Areas of titanium wear particle adhesion are highlighted. (**c**) Pin (WC) wear scar volume and wear rate for distilled water (DW) and 0.10 wt.% graphene–water (GDW). Wear rates of WC pins were calculated using abraded material volumes. Error bars are standard uncertainty.
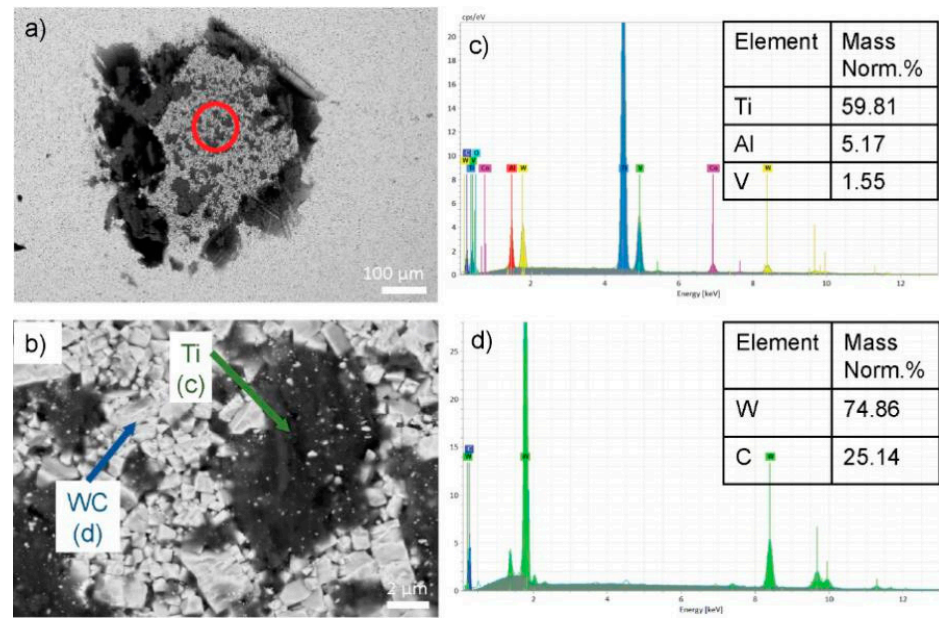
Figure 3. SEM electron backscatter images of distilled water pin wear scar (**a,b**). EDS spectrum from the Ti indicator in the SEM image (**c,d**). EDS spectrum from the WC indicator in the SEM image.

The non-monotonic friction and wear trends may be explained by the agglomeration of graphene around the contact zone, where too small a graphene concentration would not provide enough lubrication and too high a concentration prevents sliding owing to excess agglomeration of particles at the contact. It has been shown in previous studies that excess amounts of solid additives in nanofluids can negatively impact the performance of a lubricant [20,23]. Xie et al. found that excessive concentrations of graphene in water increased both the friction and wear between magnesium alloy and steel contacts: 1.0 wt.% graphene–water increased friction by 6% and the wear rate by 31% compared with the optimal concentration of 0.50 wt.% graphene–water [20]. Inferior performance above the optimal concentration is due to the agglomeration of nanoparticles around the contact zone [23]. However, none of those previous studies have investigated the tribological performance on titanium alloys. In our study of titanium alloys, we also found that an optimal graphene concentration of ~0.1 wt.% showed the best friction and wear performance. Concentrations of graphene above 0.10 wt.% likely create a larger ineffective particle that cannot easily lubricate the contact zone under high pressure. The inability of the larger graphene agglomerates to lubricate the contact zone leads to the increased friction and wear.

Wear tracks from the disk contain many galling patterns (circled in red, Figure 2a), pointing to titanium alloy being transferred to the pin during experiments. Galling is the result of friction and adhesion between sliding surfaces that causes material from one surface to stick to the other [32–34]. For all graphene concentrations we tested, the wear rates on the titanium alloy substrate were higher than the WC pin wear rates. This is to be expected as WC is much harder than Ti alloy. Hardness is often viewed as a measure of abrasive wear resistance. WC has a Vickers hardness of 1550 kgf/mm^2, while Ti alloy (grade 5) has a Vickers hardness of 349 kgf/mm^2. Ti is also quite prone to adhesive wear thanks to its reactivity and high stacking fault energy [33,34].

3.2. Effect of Surface Roughness on Friction

Friction and wear are usually affected by the surface roughness. In our research, we also studied the effect of substrate surface roughness on friction with different concentrations of graphene, as shown in Figure 4a. Overall, the 0.10 wt.% graphene concentration shows a low average friction coefficient and wear for the range of surface roughness tested. The highest surface roughness, 1.02 μm, had the lowest COF and wear, with graphene concentrations of 0.10 and 0.15 wt% showing comparable improvements. Figure 4b shows the friction coefficient as a function of time with 0.10 wt.% graphene lubricant on three different roughness surfaces: 0.08 μm, 0.51 μm, and 1.02 μm. Figure 4c–e shows SEM images of the post-experiment wear tracks for 0.10 wt.% graphene with different surface roughness values.

Previous studies on nanofluid lubricants have found different trends of friction and wear with surface roughness. Gara and Zou found that increasing the surface roughness (Ra) from 25 nm to 240 nm increased friction by 12% with 1 wt.% ZnO and oleic acid in paraffin oil on steel–steel contacts during pin-on-disk tests [35]. In contrast, it was also reported in a previous study that greater surface roughness values could result in lower friction and wear, depending on the size of the nanoparticles in the nanofluid [36]. It was found that the nanoparticles must be smaller, but not too much smaller, than the average surface roughness to see the greatest friction and wear reduction. If the nanoparticles were too small (<0.1 μm), a much larger agglomeration would occur, creating an effective particle size over a micron in diameter. These observations are consistent with our results even though the substrate materials and lubricants differ between the two studies.
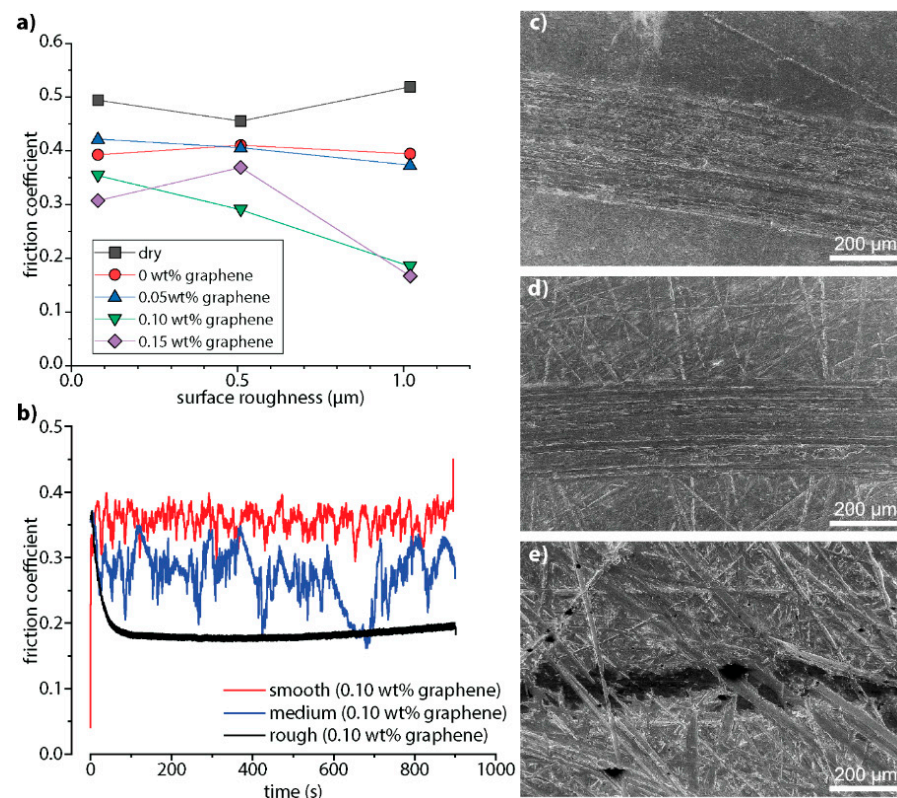
Figure 4. (**a**) Coefficient of friction for disk surface roughness of 0.08 μm, 0.51 μm, and 1.02 μm. Values given for various concentrations of graphene nanoflakes in distilled water. Error bars are standard deviation. Friction coefficient vs. time for 0.10 wt.% graphene against smooth (0.08 μm), medium (0.51 μm), and rough (1.02 μm) Ti6Al4V surfaces. (**b**) The friction coefficient as a function of time with 0.10 wt.% graphene lubricant on three different surface roughness: 0.08 μm, 0.51 μm, and 1.02 μm. SEM images of disk wear track for 0.10 wt.% graphene-water experiments with variable surface roughness: (**c**) 0.08 μm, (**d**) 0.51 μm, and (**e**) 1.02 μm.

Many mechanisms have been proposed for how graphene nanofluids (or other additives) lubricate a surface. These include the following: the deformed additive sheets act as ball bearings and introduce rolling friction, nanomaterials form an interface layer or tribofilm, filling in valleys and grooves on a rough surface, and additives cause micropolishing that creates smoother surfaces. Owing to the quick sedimentation of graphene in distilled water with no surfactant, the graphene nanoparticles are likely falling out of solution during the tests. The graphene nanoparticles likely fill up the troughs in the rough titanium alloy surface. As rougher surfaces have deeper scratches and more variation, the graphene particles have a greater volume to occupy near the surface. The increased presence of graphene in the contact zone may increase the probability of the pin sliding over a smoother graphene surface rather than the rough titanium surface. This mechanism agrees with the experimental results in the Peña-Parás et al. study, as well as the results of this study when nanofluid solutions are tested against rough surfaces [30]. In this study, the roughest surface (1.02 μm) saw reduced friction (μ < 0.2) and wear from the larger effective particle size created from the agglomerations of the 0.10 and 0.15 wt.% graphene–water nanofluids. Figure 4b shows the roughest surface had a consistent low COF contrasted to the large swings seen on the smoother surfaces. The likely graphene agglomerations that formed on the titanium surface were too large to effectively fill the valleys on the surface of the 0.08 and 0.51 μm Ra surfaces. The lack of graphene available at the interface likely leads to higher friction and wear compared with the rougher surface, which had a larger concentration of graphene available. Figure 5 shows the proposed mechanism for graphene lubricating a rough surface more effectively than a smooth surface. Given two

surfaces, one with a surface roughness of 0.5 μm and the other with a surface roughness of 1.0 μm, graphene (represented as a plate) will deform more on the 1.0 μm surface under an evenly applied pressure. This is because of the larger area between asperity peaks (acting as supports) on the rough surface. The increased deformation allows graphene to fill in troughs and remain on the rough surface more effectively than a smooth surface. Over time, graphene on the rough surface will accumulate with each pass of the pin, reducing friction and wear by reducing direct contact between the pin and disk surfaces. For a smoother surface over time, as a result of less deformation, graphene does not easily remain on the surface and struggles to create a stable, protective film, which increases friction and wear.
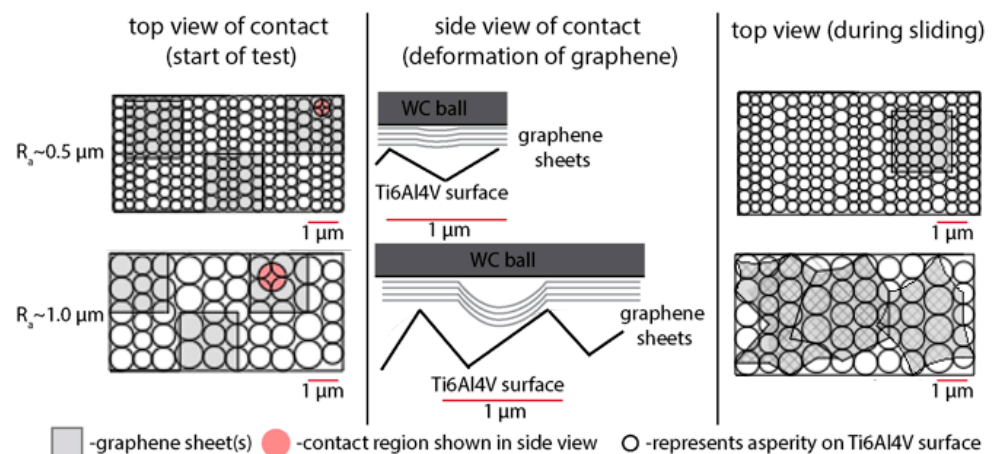
Figure 5. Mechanistic description of the effect of surface roughness on graphene nanofluid lubrication. Initially (LHS of figure), graphene sheets sit on top of the Ti-6Al-4V surface. Then, the contact pressure due to the WC ball causes the graphene sheets to conform to the surface (middle figure). Owing to the larger unsupported distance for rougher surfaces, the graphene sheets are more likely to undergo larger deformation and may buckle. These buckled sheets are more likely to stay in the contact, as they are no longer entirely 2D (RHS of figure). With additional graphene in the contact region, the WC–Ti contact area and friction coefficient are reduced (cf., Figure 4b).

4. Conclusions

This study investigates the tribological performance of water-based graphene nanofluids on Ti and WC contact pairs. These graphene nanofluids are found to reduce friction and wear, but this depends on the concentration and surface roughness. A non-monotonic trend is observed for graphene concentrations between 0 and 0.25 wt.%; a 0.10 wt.% graphene concentration is optimal on a 0.51 μm Ra surface, reducing friction and pin wear by 37% and 95% compared with water alone.

Surface roughness of the titanium disk affects the nanofluid performance. Between three surface profiles, the highest (roughest; 1.02 μm) Ra value has the lowest friction and wear. Friction is consistently low on these rough surfaces with large (0.10 wt.% and greater) graphene concentrations, while friction is higher and more variable with smother surfaces at the same concentrations.

This tribological behavior is attributed to graphene nanoparticle agglomerations and their size relative to surface roughness. A mechanism is proposed in which rough surfaces (with large asperities) allow higher concentrations (with large nanoparticle agglomerations) to lubricate more effectively owing to the formation of stable, protective graphene films. Each surface roughness value will have an optimal concentration. Too high a concentration used on a relatively smooth surface will see increased friction and wear, as the large nanoparticle agglomerations struggle to remain in the contact zone and create a film. These results give insight into the mechanics of lubrication with graphene–water nanolubricants and their interaction with sample surface roughness. Further work needs to be undertaken, however, to fully investigate these hypotheses and understand graphene's unique behavior.

References

1. Veiga, C.; Davim, J.P.; Loureiro, A.J.R. Review on machinability of titanium alloys: The process perspective. *Rev. Adv. Mater. Sci.* **2013**, *34*, 148–164.
2. Ezugwu, E.O.; Wang, Z.M. Titanium alloys and their machinability—A review. *J. Mater. Process. Technol.* **1997**, *68*, 262–274. [CrossRef]
3. Rahman, M.; Wang, Z.G.; Wong, Y.S. An overview of high-speed machining of titanium alloys. In Proceedings of the LEM 2005-3rd International Conference on Leading Edge Manufacturing 21st Century, Nagoya, Japan, 19–22 October 2005; Volume 49, pp. 19–28.
4. Arrazola, P.J.; Garay, A.; Iriarte, L.M.; Armendia, M.; Marya, S.; le Maître, F. Machinability of titanium alloys (Ti6Al4V and Ti555.3). *J. Mater. Process. Technol.* **2009**, *209*, 2223–2230. [CrossRef]
5. Zareena, A.R.; Veldhuis, S.C. Tool wear mechanisms and tool life enhancement in ultra-precision machining of titanium. *J. Mater. Process. Technol.* **2012**, *212*, 560–570. [CrossRef]
6. Abdel-Aal, H.A.; Nouari, M.; El Mansori, M. Influence of thermal conductivity on wear when machining titanium alloys. *Tribol. Int.* **2009**, *42*, 359–372. [CrossRef]
7. Pramanik, A. Problems and solutions in machining of titanium alloys. *Int. J. Adv. Manuf. Technol.* **2014**, *70*, 919–928. [CrossRef]
8. Soković, M.; Mijanović, K. Ecological aspects of the cutting fluids and its influence on quantifiable parameters of the cutting processes. *J. Mater. Process. Technol.* **2001**, *109*, 181–189. [CrossRef]
9. Sharma, A.K.; Tiwari, A.K.; Dixit, A.R. Effects of Minimum Quantity Lubrication (MQL) in machining processes using conventional and nanofluid based cutting fluids: A comprehensive review. *J. Clean. Prod.* **2016**, *127*, 1–18. [CrossRef]
10. Wang, X.Q.; Mujumdar, A.S. Heat transfer characteristics of nanofluids: A review. *Int. J. Therm. Sci.* **2007**, *46*, 1–19. [CrossRef]
11. Taha-Tijerina, J.; Peña-Paras, L.; Narayanan, T.N.; Garza, L.; Lapray, C.; Gonzalez, J.; Palacios, E.; Molina, D.; García, A.; Maldonado, D.; et al. Multifunctional nanofluids with 2D nanosheets for thermal and tribological management. *Wear* **2013**, *302*, 1241–1248. [CrossRef]
12. Chen, Y.; Hu, E.; Zhong, H.; Wang, J.; Subedi, A.; Hu, K.; Hu, X. Characterization and Tribological Performances of Graphene and Fluorinated Graphene Particles in PAO. *Nanomaterials* **2021**, *11*, 2126. [CrossRef] [PubMed]
13. Mao, J.; Chen, G.; Zhao, J.; He, Y.; Luo, J. An investigation on the tribological behaviors of steel/copper and steel/steel friction pairs via lubrication with a graphene additive. *Friction* **2021**, *9*, 228–238. [CrossRef]
14. del Río, J.M.L.; López, E.R.; Fernández, J. Tribological properties of graphene nanoplatelets or boron nitride nanoparticles as additives of a polyalphaolefin base oil. *J. Mol. Liq.* **2021**, *333*, 115911. [CrossRef]
15. Yu, W.; Xie, H.; Wang, X.; Wang, X. Significant thermal conductivity enhancement for nanofluids containing graphene nanosheets. *Phys. Lett. Sect. A Gen. At. Solid State Phys.* **2011**, *375*, 1323–1328. [CrossRef]
16. Berman, D.; Erdemir, A.; Sumant, A.V. Graphene: A new emerging lubricant. *Mater. Today* **2014**, *17*, 31–42. [CrossRef]
17. Sattari Baboukani, B.; Ye, Z.; GReyes, K.; Nalam, P.C. Prediction of nanoscale friction for two-dimensional materials using a machine learning approach. *Tribol. Lett.* **2020**, *68*, 1–14. [CrossRef]
18. Gong, P.; Egberts, P. Influence of heating on the measured friction behavior of graphene evaluated under ultra-high vacuum conditions. *Appl. Phys. Lett.* **2021**, *119*, 063102. [CrossRef]
19. Li, P.F.; Zhou, H.; Cheng, X.H. Nano/micro tribological behaviors of a self-assembled graphene oxide nanolayer on Ti/titanium alloy substrates. *Appl. Surf. Sci.* **2013**, *285*, 937–944. [CrossRef]
20. Xie, H.; Jiang, B.; Dai, J.; Peng, C.; Li, C.; Li, Q.; Pan, F. Tribological behaviors of graphene and graphene oxide as water-based lubricant additives for magnesium alloy/steel contacts. *Materials* **2018**, *11*, 206. [CrossRef]
21. Kinoshita, H.; Nishina, Y.; Alias, A.A.; Fujii, M. Tribological properties of monolayer graphene oxide sheets as water-based lubricant additives. *Carbon* **2014**, *66*, 720–723. [CrossRef]
22. Eswaraiah, V.; Sankaranarayanan, V.; Ramaprabhu, S. Graphene-based engine oil nanofluids for tribological applications. *ACS Appl. Mater. Interfaces* **2011**, *3*, 4221–4227. [CrossRef] [PubMed]
23. Mungse, H.P.; Khatri, O.P. Chemically functionalized reduced graphene oxide as a novel material for reduction of friction and wear. *J. Phys. Chem. C* **2014**, *118*, 14394–14402. [CrossRef]

24. Li, M.; Yu, T.; Yang, L.; Li, H.; Zhang, R.; Wang, W. Parameter optimization during minimum quantity lubrication milling of TC4 alloy with graphene-dispersed vegetable-oil-based cutting fluid. *J. Clean. Prod.* **2019**, *209*, 1508–1522. [CrossRef]

25. Yi, S.; Li, G.; Ding, S.; Mo, J. Performance and mechanisms of graphene oxide suspended cutting fluid in the drilling of titanium alloy Ti-6Al-4V. *J. Manuf. Process.* **2017**, *29*, 182–193. [CrossRef]

26. Liang, S.; Shen, Z.; Yi, M.; Liu, L.; Zhang, X.; Ma, S. In-situ exfoliated graphene for high-performance water-based lubricants. *Carbon* **2016**, *96*, 1181–1190. [CrossRef]

27. Zhang, J.; Li, P.; Zhang, Z.; Wang, X.; Tang, J.; Liu, H.; Shao, Q.; Ding, T.; Umar, A.; Guo, Z. Solvent-free graphene liquids: Promising candidates for lubricants without the base oil. *J. Colloid Interface Sci.* **2019**, *542*, 159–167. [CrossRef] [PubMed]

28. Burris, D.L.; Sawyer, W.G. Measurement uncertainties in wear rates. *Tribol. Lett.* **2009**, *36*, 81–87. [CrossRef]

29. Colbert, R.S.; Krick, B.A.; Dunn, A.C.; Vail, J.R.; Argibay, N.; Sawyer, W.G. Uncertainty in pin-on-disk wear volume measurements using surface scanning techniques. *Tribol. Lett.* **2011**, *42*, 129–131. [CrossRef]

30. Schmitz, T.L.; Action, J.E.; Burris, D.L.; Ziegert, J.C.; Sawyer, W.G. Wear-Rate Uncertainty Analysis. *J. Tribol.* **2004**, *126*, 802. [CrossRef]

31. Erickson, G.M.; Sidebottom, M.A.; Curry, J.F.; Kay, D.I.; Kuhn-Hendricks, S.; Norell, M.A.; Sawyer, W.G.; Krick, B.A. Paleo-tribology: Development of wear measurement techniques and a three-dimensional model revealing how grinding dentitions selfwear to enable functionality. *Surf. Topogr. Metrol. Prop.* **2016**, *4*, 024001. [CrossRef]

32. Podgornik, B.; Hogmark, S. Surface modification to improve friction and galling properties of forming tools. *J. Mater. Process. Technol.* **2006**, *174*, 334–341. [CrossRef]

33. Bhansali, K.J.; Miller, A.E. The role of stacking fault energy on galling and wear behavior. *Wear* **1982**, *75*, 241–252. [CrossRef]

34. Lebedeva, I.L.; Presnyakova, G.N. Adhesion wear mechanisms under dry friction of titanium alloys in vacuum. *Wear* **1991**, *148*, 203–210. [CrossRef]

35. Gara, L.; Zou, Q. Friction and wear characteristics of oil-based ZnO nanofluids. *Tribol. Trans.* **2013**, *56*, 236–244. [CrossRef]

36. Peña-Parás, L.; Gao, H.; Maldonado-Cortés, D.; Vellore, A.; García-Pineda, P.; Montemayor, O.E.; Nava, K.L.; Martini, A. Effects of substrate surface roughness and nano/micro particle additive size on friction and wear in lubricated sliding. *Tribol. Int.* **2018**, *119*, 88–98. [CrossRef]